CrossMark

Microstructure, Fatigue Behavior, and Failure Mechanisms of Direct Laser-Deposited Inconel 718

ALEX S. JOHNSON,[1] SHUAI SHAO,[1] NIMA SHAMSAEI,[2,4]
SCOTT M. THOMPSON,[2] and LINKAN BIAN[3]

1.—Center for Advanced Vehicular Systems (CAVS), Mississippi State University, Starkville, MS 39759, USA. 2.—Department of Mechanical Engineering, Auburn University, Auburn, AL 36849, USA. 3.—Department of Industrial and Systems Engineering, Mississippi State University, Starkville, MS 39762, USA. 4.—e-mail: shamsaei@auburn.edu

Inconel 718 is considered to be a superalloy with a series of superior properties such as high strength, creep resistance, and corrosion resistance at room and elevated temperatures. Additive manufacturing (AM) is particularly appealing to Inconel 718 because of its near-net-shape production capability for circumventing the poor machinability of this superalloy. Nevertheless, AM parts are prone to porosity, which is detrimental to their fatigue resistance. Thus, further understanding of their fatigue behavior is required before their widespread use in load-bearing applications. In this work, the microstructure and fatigue properties of AM Inconel 718, produced in a Laser Engineered Net Shaping (LENS^{TM}) system and heat treated with a standard heat treatment schedule, are evaluated at room temperature. Fully reversed strain controlled fatigue tests were performed on cylindrical specimens with straight gage sections at strain amplitudes ranging from 0.001 mm/mm to 0.01 mm/mm. The fracture surfaces of fatigue specimens were inspected with a scanning electron microscope. The results indicate that the employed heat treatment allowed the large, elongated grains and dendritic structure of the as-built material to break down into smaller, equiaxed grains, with some dendritic structures remaining between layers. The AM specimens were found to possess lower fatigue resistance than wrought Inconel 718, and this is primarily attributed to the presence of brittle metal-carbide/oxide inclusions or pores near their surface.

List of abbreviations

$2N_f$	Reversals to failure
AM	Additive manufacturing
b	Fatigue strength exponent
BD	Build direction
c	Fatigue ductility exponent
E	Elastic modulus
EDS	Energy-dispersive x-ray spectroscopy
LENS	Laser Engineered Net Shaping
R^2	Coefficient of determination
SEM	Scanning electron microscope
$\frac{\Delta\varepsilon}{2}$	Total strain amplitude
ε_f'	Fatigue ductility coefficient
σ_f'	Fatigue strength coefficient

INTRODUCTION

Inconel 718 is a precipitation-hardened, nickel-based super alloy that, because of its retention of strength in harsh environments,[1] has been used with success by manufacturers in many extreme-temperature aerospace applications, such as for turbine blades in jet engines, liquid-fueled rocket components, and cryogenic containers. Inconel alloys are well known for their toughness and difficulty to machine.[1–3] To circumvent a large portion of machining and preparation time, additive manufacturing (AM), which produces parts in a cumulative, layer-by-layer fashion, can help produce near net-shape, metallic parts. The AM process also allows for a wider and more complex range of part geometries to be produced relative to typical subtractive manufacturing and casting.

The use of AM for application-worthy part production is not without its drawbacks or risks.[4,5] For instance, the process can induce porosity (spherical or slit-shaped) and inclusions and, thus, stress concentrations in the material structure, which is detrimental to a final part's mechanical integrity, especially under fatigue loading conditions. Such defects result either from non-fully-optimized

processing parameters or from the employment of low-quality feedstock (e.g., powder, wire). In addition, the AM process is conducive for epitaxial and elongated grain growth along the build and major thermal gradient directions, giving rise to anisotropy in the mechanical properties of the part.[6] Therefore, the production of application-worthy parts becomes problematic as both process and feedstock-driven defects, as well as inconsistencies in the part microstructure, can lead to unpredictable mechanical behavior, especially in its fatigue response.[7] Hence, it is pivotal that the performance of AM metals be further understood and correlated to specific AM processing conditions and encumbered microstructures.

In general, fatigue accounts for a big potion of mechanical failures;[8] thus, understanding the fatigue behavior and other mechanical properties of AM Inconel is of utmost importance. To date, most fatigue research on Inconel 718 has centered on its traditionally manufactured form.[9–16] In both the low-cycle and high-cycle fatigue regimes, cracks typically initiate from transgranular slip bands at or near the surface of specimens and grow to up to 50 μm in the short crack regime before transitioning to the long crack regime and growing through 60–70% of the specimen's cross-sectional area to the final fracture.[9,15] Most crack growth has been found to be of a transgranular, faceted mode.[9–12,16]

Some recent work has been focused on the mechanical performance of AM nickel-based super alloys, including AM Inconel 718. Amsterdam and Kool[7] experimentally investigated the fatigue performance of AM Inconel 718 under load control conditions at room temperature. Although most AM and wrought specimen performance data correlated well, some AM specimens showed lives orders-of-magnitude shorter at comparable stresses, specifically in the high-cycle fatigue regime. Interestingly, macro-sized pores were found to have little effect on the fatigue behavior of the AM material, whereas lack of bonding/fusion vacancies were found to be more contributive to the reduced fatigue performance.[7]

Although significant research has been conducted on the load-controlled, high-cycle fatigue behavior of Inconel 718, there is very little data describing its strain-controlled fatigue behavior. To the best of the authors' knowledge, there are no strain-controlled fatigue data, covering both low- and high-cycle life regimes, available in the open literature for AM Inconel 718. Therefore, this study was aimed at investigating the fatigue behavior of AM Inconel 718 via strain-controlled fatigue tests, with a focus on elucidate structure–property relationships inherent to AM Inconel 718. The effects of heat treatment on the microstructure of the material is examined. The strain-life fatigue data are obtained and compared with existing data on wrought Inconel. The specimen fracture surfaces are inspected to understand the micro-mechanisms involved in fatigue crack initiation and propagation within AM Inconel 718.

EXPERIMENTAL PROCEDURE

The specimens were additively manufactured with an argon-purged OPTOMEC LENS$^{\text{TM}}$ 750 system. Plasma electrode rotation prepared (PREP) Inconel 718 powder with granule size ranging from 45 to 150 μm is used to fabricate all specimens. To ensure dense, near net-shape parts, six tracks of preliminary linear cladding tests $\sim$5 cm in length were deposited and then sectioned to inspect their cross-sectional shape and degree of fusion with the substrate. An optimum set of process parameters, i.e., laser power of 350 W, scan speed of 15 mm/s, powder flow rate of 0.057 g/s, and hatch spacing of 0.529 mm, was determined and used for manufacturing 21 cylindrical rod specimens. All specimens were built one at a time on the same wrought Inconel 718 substrate, each spaced approximately 75 mm apart.

All of the as-fabricated AM parts were removed from the substrate and machined into round fatigue specimens according to ASTM Standard E606[17] for testing, except one that remained unmachined for inspection of its microstructure. The gage section of each specimen was machined to a length of 15 mm and a diameter of 3.5 mm. The grip sections were each 27 mm long with a diameter of 7 mm. The shoulder radius between the grip and gage sections was 10 mm. Fatigue tests were conducted at room temperature in an ambient lab atmosphere, which was $\sim$24°C $\pm$ 2°C at $\sim$40% humidity. All specimens were subject to the standard heat treatment for Inconel 718: 940°C for 2 h followed by out-of-furnace air cooling, aging at 718°C for 8 h followed by cooling at a rate of 50°C/h to 621°C, and held at this temperature for another 8 h followed by air cooling.[16]

Both heat-treated and as-built specimens were sectioned, mounted, and polished for microstructure analysis. Etching was accomplished with Waterless Kalling's etchant. Fully reversed strain-controlled fatigue tests were performed on a MTS Landmark system at strain amplitudes of 0.01 mm/mm, 0.008 mm/mm, 0.006 mm/mm, 0.005 mm/mm, 0.004 mm/mm, 0.003 mm/mm, 0.002 mm/mm, and 0.001 mm/mm. At least two tests were performed at each strain level except for 0.001 mm/mm as a result of being runout. Before testing, the gage sections of all specimens were polished along the loading direction to remove circumferential surface machining marks. After failure, fracture surfaces were cut from the fatigue specimens and examined via scanning electron microscopy (SEM). Energy-dispersive x-ray spectrometry (EDS) was used to investigate the crack initiation points, once located.

EXPERIMENTAL RESULTS AND DISCUSSION

Microstructure Properties

To examine the microstructures of the as-built and heat-treated specimens, each specimen was sectioned into segments consisting of the grip

section and the gage section. These sections were cut in half longitudinally, i.e., Sections B and C in Fig. 1, respectively, to view the inner sections of the specimens. For the heat-treated sections, a circular cross section of the substrate-sided grip section was also examined, i.e., Section A. The gage section of the as-built specimen was found to contain large and elongated grains (Fig. 1a, average of ~170 μm in size along the elongated direction), with variation in grain size and faint dendritic structure within the grains, as seen in the lower half of Fig. 1a.

After heat treatment, small portions of dendritic structures, specific to the AM process,[18–22] remained in the gage section (Fig. 1b, circled). After heat treatment, most of the large, elongated grains initially present in the as-built gage section (Fig. 1a) were found to recrystallize and form smaller, equiaxed grains (Fig. 1b) consistent with the results of Zhao et al.[18] and Liu et al.[19] The average grain size at the heat-treated gage section was found to be ~43 μm. A clear interlayer fusion zone, characterized by smaller and randomly shaped grains containing dendrites, which interrupts the normal microstructural consistency, seems to persist even after the heat treatment, as seen between dashed lines in Fig. 1a and b.

Lack of fusion between layers is found to be prevalent in the first several layers deposited near the substrate (section A, Fig. 1c). This lack of fusion
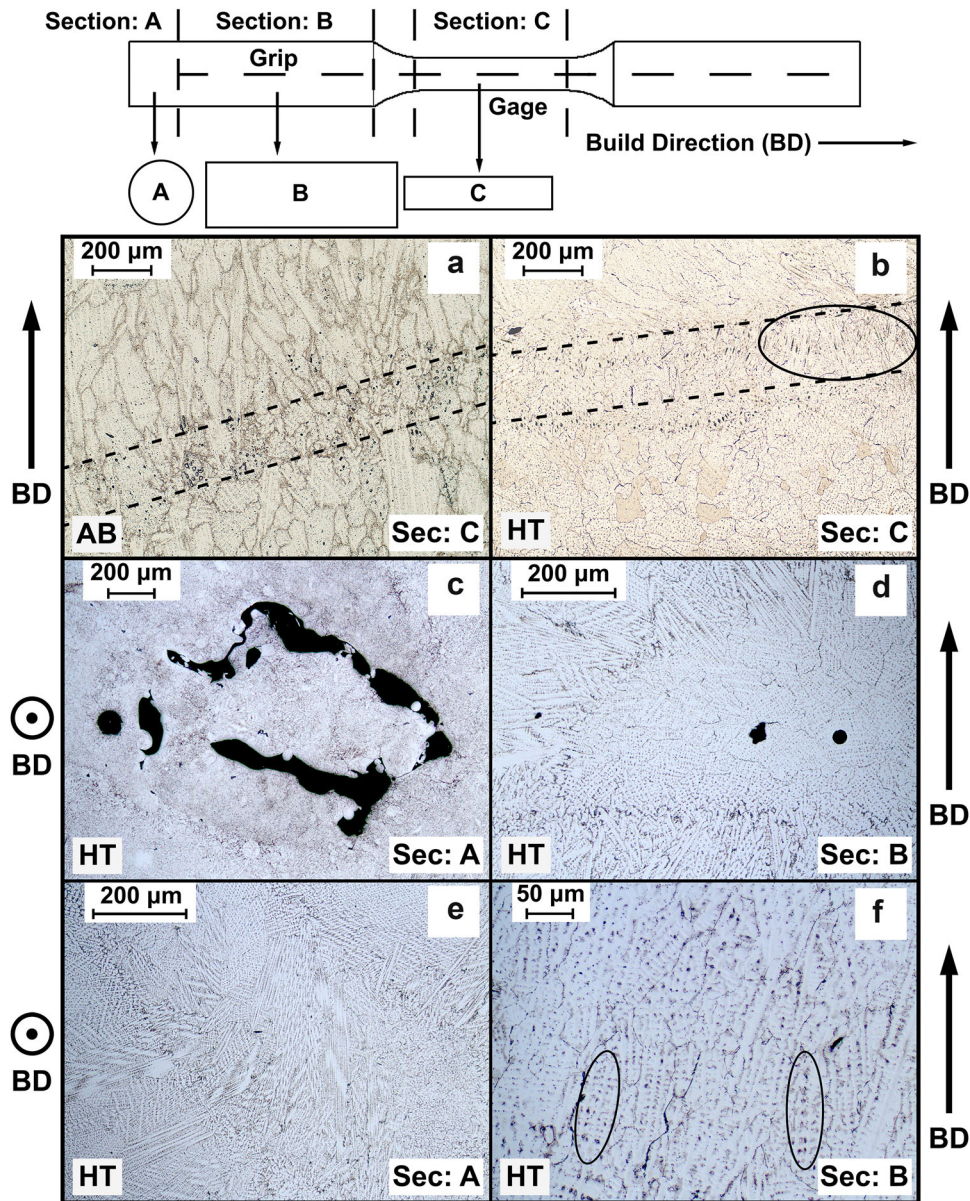

Fig. 1. Sectioning diagram and microstructure of heat-treated and as-built AM Inconel 718 specimens. (a) Microstructure of as-built gage section. (b) Microstructure of heat-treated gage section. Regions inside dashed lines are fusion zones between layers. (c) Circular cross section of heat-treated grip section near substrate (Section A). (d) Microstructure of heat-treated grip section showing pores. (e) Residual dendritic structure in heat-treated specimen (Section A). (f) Magnified view of the heat-treated grip section (Section B).

between the substrate and early deposited layers was also reported to occur in the "cross-bonded" specimens presented in Blackwell's work.[20] These defects are most likely a result of higher cooling rates along the non-preheated substrate interplaying with the instability of the melt pool. As the build gets further away from the substrate, the previously deposited layers retain more heat and allow for better fusion of subsequent layers. Therefore, in the gage section, only small spherical pores with a diameter less than 45 μm exist, as seen in Fig. 1d. This is in agreement with Zhao et al.,[18] where pore sizes from 25 μm to 70 μm were observed. As large amounts of porosity and lack of fusion tend to occur in the layers near the base of the build (Fig. 1c), it is recommended that critical structural portions of parts be built in layers further away from the substrate, with part portions near the substrate deemed sacrificial in nature.

The microstructures of specimen regions located near the substrate were found to be mainly composed of a dendritic structure even after heat treatment, as seen in Fig. 1e. More dendrites near the substrate are most likely caused by erratic, localized, and instantaneous cooling rates occurring during the solidification of deposited material.[18–21] Further from the substrate after heat treatment, the dendrites become more dissolved into the more equiaxed grain structure. An interesting characteristic is presented in Fig. 1f, as was explained by Qi et al.;[22] the spotted pattern observed (Fig. 1f circled, and Fig. 1b, lower grains) within grains is likely residual interdendritic Laves phases left over from the heat treatment process. During the employed heat treatment, most of the Laves phases did dissolve into the matrix or transformed into the δ phase. The solution annealing temperature was likely not sufficiently high for fully dissolving these phases back into the material matrix.[22]

The unique processing path of the AM Inconel 718 produces microstructures distinct from their wrought counterparts. Directionally oriented dendritic and grain structures, porosity, and lack of fusion are several of the unique features observed in the AM specimens. Because the dendritic microstructure appears not to dissolve fully during the heat treatment process, areas of residual dendritic microstructure may influence mechanical properties. Properly adapting a heat treatment process specifically for homogenizing the grains in AM Inconel 718 could remedy this issue. Porosity and lack of fusion can be minimized by proper parameters used in manufacturing the specimens.

Fatigue Properties

The Coffin–Manson equation is defined as the sum of the elastic, $\frac{\sigma_f'}{E}(2N_f)^b$, and plastic, $\varepsilon_f'(2N_f)^c$, portions of total strain amplitude, $\frac{\Delta\varepsilon}{2}$:[8]

$$\frac{\Delta\varepsilon}{2} = \frac{\sigma_f'}{E}(2N_f)^b + \varepsilon_f'(2N_f)^c \tag{1}$$

where σ_f' is the fatigue strength coefficient, E is the modulus of elasticity, $2N_f$ is the reversals to failure, b is the fatigue strength exponent, ε_f' is the fatigue ductility coefficient, and c is the fatigue ductility exponent. Figure 2a presents the elastic, plastic, and total strain amplitudes versus fatigue lives data and fits. The fitted parameters are σ_f' = 2090 MPa, $b = -0.111$, ε_f' = 1.8 mm/mm, and $c = -0.775$. Tests with very small plastic deformation were excluded from the calculations. It may be noted that collected data follow a smooth, consistent curve with little scatter, as indicated by $R^2 = 0.96$.

The fatigue data for wrought Inconel 718 reported by Brinkman and Korth[16] are presented in Fig. 2b and compared against the AM data generated herein. Note that the heat treatment process used in both studies was the same. The results demonstrate that the fatigue lives of AM specimens in this study are shorter than those of their wrought counterparts. In the high-cycle fatigue regime, the
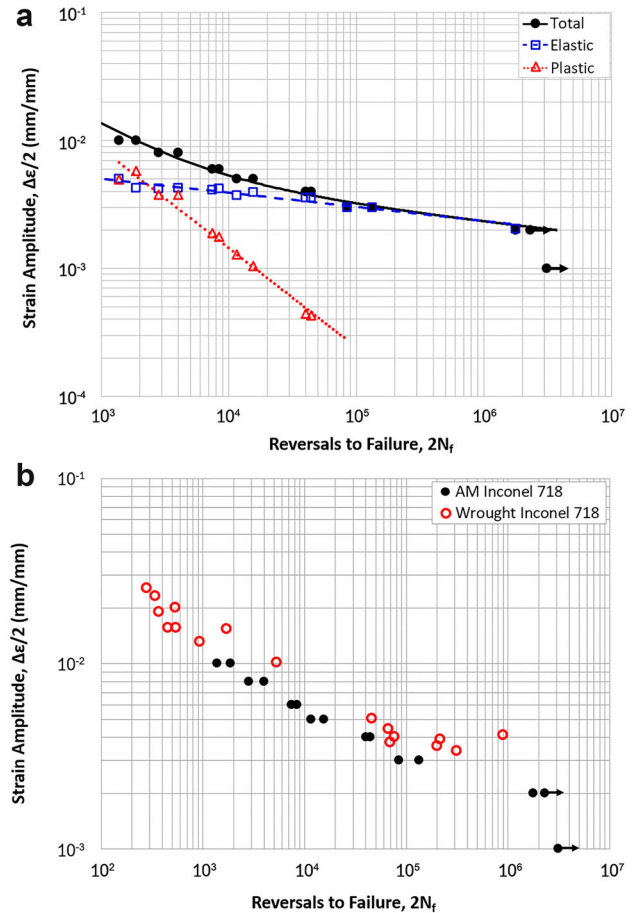

Fig. 2. (a) Total, elastic, and plastic strain amplitudes versus fatigue lives data and fits for AM Inconel 718 specimens in this study. (b) Strain-life fatigue behavior of AM Inconel 718 and its comparison to wrought Inconel 718.[16] Arrows indicate runout tests.

AM specimens were found to possess even shorter fatigue lives (up to an order-of-magnitude) relative to wrought specimens. As will be discussed in more detail later, AM defects are most likely the major cause for the reduced fatigue life.

Fractography

SEM analysis of the resulting fracture surfaces reveals insights into the fatigue behavior of the AM Inconel 718 specimens. Representative fracture surfaces obtained from fatigue tests in high- and low-cycle regimes are presented in Figs. 3 and 4, respectively. All specimens exhibited distinct crack growth and final fracture regions. Crack growth regions are observed by fine striations (Fig. 3c and right box in Fig. 4b) running perpendicular to the crack growth direction (dashed arrows in Figs. 3 and 4). The final fracture regions are distinguished by the high amount of dimpling on the fracture surface (Fig. 3b), indicating ductile final fracture behavior. Most crack growth regions are generally flat and of transgranular mode with clear river-marks (Fig. 3d, solid arrows) running back toward the initiation point (Fig. 3d, circled). The general fracture surface features mentioned earlier mirror those reported by Amsterdam and Kool,[7] whom also investigated AM Inconel 718.

Many exposed pores can be observed on the high-cycle and low-cycle fatigue fracture surfaces in Fig. 3b and c and Fig. 4f, as marked by solid black arrows. Inclusion particles also appear on the fracture surfaces as observed in Fig. 4b and d (circled). These particles are in the range of 10–20 μm in length but have different shapes. These surface or near-surface particles served as crack initiation sites for several fatigue specimens investigated herein. For specimens in the high-cycle regime, no pores were found to accompany particles seen in initiation zones. EDS was implemented to investigate the nature of the particles. In Fig. 4, the numbered particles in circles were identified to be (1) carbide, (2) magnesium oxide, and (3) aluminum oxide particles, respectively.

A few of the fracture surfaces were also found to have pores, between 1 μm and 3 μm in size, in near proximity to the surface that initiated the crack, like those observed in the initiation region of Fig. 4e and magnified in Fig. 4f (top arrow). The amount of exposed pores in this area indicates that they may have played a role in early crack initiation. Areas around the pores were analyzed via EDS and found to contain a high amount of carbon. The area around the lower left pore contained a high amount of boron, which is known to enhance the low-cycle fatigue life of nickel alloys.[23] Therefore, the pore
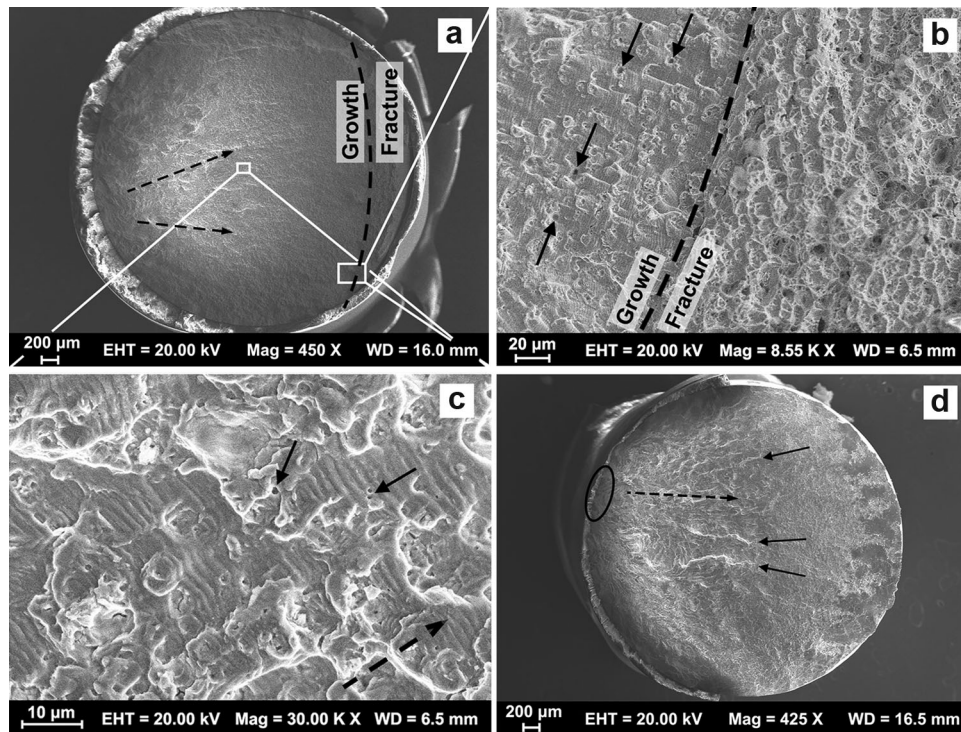

Fig. 3. Fatigue fracture surfaces of AM Inconel 718 from high-cycle fatigue tests. Crack growth directions marked by dashed arrows. (a) Fracture surface of a 0.003-mm/mm strain amplitude test, final fracture region to the right of the dashed line. (b) Transition from crack growth to final fracture (indicated by dashed arc), larger exposed pores indicated by solid arrows. (c) Magnified view of notable striations present on crack growth region, as well as exposed pores indicated by solid arrows. (d) Example of river marks (indicated by solid arrows) for a 0.002-mm/mm strain amplitude test leading back toward the initiation site (circled).
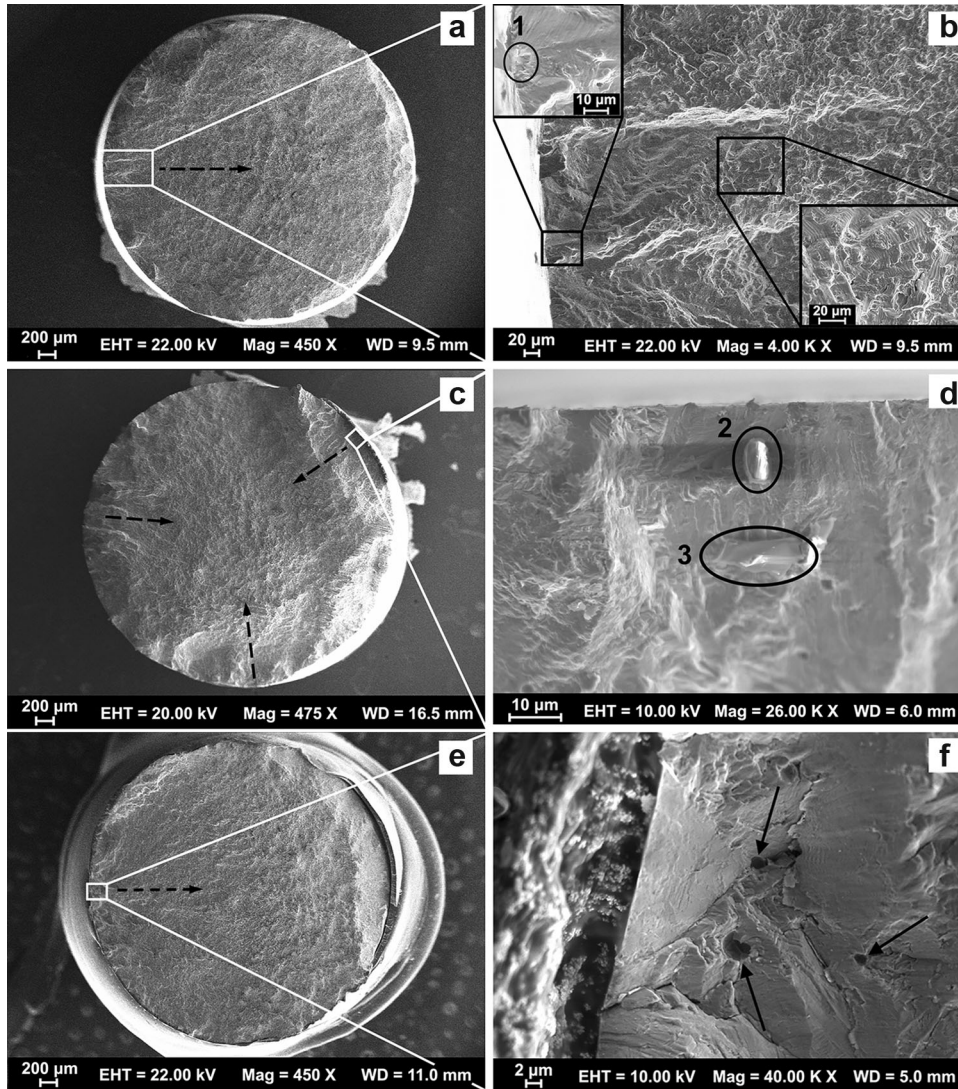
Fig. 4. Fatigue fracture surfaces of AM Inconel 718 from low-cycle fatigue tests. Crack growth directions marked by dashed arrows. (a) and (b) Fracture surface of a 0.01-mm/mm strain amplitude test. (b) Initiation area boxed and magnified on the left of (b). Initiation of the crack (circled). Striations near initiation region (boxed, right). (c) and (d) Fracture surface of a 0.006-mm/mm strain amplitude test. (d) Crack initiation region, where two near-surface particles acted as crack initiators (circled). (e) and (f) Another 0.006-mm/mm strain amplitude test. (f) Crack initiation region, solid arrows indicate pores at the crack initiation site.

surrounded by the carbon laden region is most likely responsible for crack initiation as a result of its brittleness relative to the material matrix.

Such defects, pores, and inclusion particles, as shown in Fig. 4b, d, and f, are possibly sourced from the employed LENS process and feedstock, and are likely the cause of the reduced fatigue performance observed in Fig. 2b as a result of the modulus mismatch between the particles and material matrix. When these particles/or pores exist near the surface of the specimen, they accelerate the initiation of fatigue cracks caused by local stress concentrations. Careful attention must be taken with contaminants in the AM machines and in handling the powder for preventing such particle intrusion. Exclusion of these particles may result in an increase in the

fatigue lives of the AM materials. The challenge then centers on how to prevent contamination during the build process or stopping elements in the alloy from segregating to form particles.

CONCLUSION

The microstructure, fatigue life, and failure mechanisms of additive manufactured (AM) Inconel 718 alloy have been investigated. LENS samples were conventionally heat treated and tested under strain-controlled fatigue loadings. The following conclusions can be drawn:

1. As-built AM Inconel 718 specimens typically have elongated grains in the build direction, as well as large amounts of the dendritic structure.

Lack-of-fusion pores can exist near the substrate, whereas spherical pores exist away from the substrate.

2. Conventional heat treatment of AM Inconel 718 specimens can create a smaller and more uniform grain structure; nevertheless, it cannot completely dissolve dendrites and the interdendritic Laves phase. The δ phase may also form during heat treatment as a result of the breakdown of the dendritic structures.

3. Although the fatigue lives of AM Inconel 718 are more comparable to those of wrought in the short life regime, they can be an order of magnitude shorter than the wrought counterpart in the long life regime.

4. Cracks originate from hard particles or pores at or near the surface in AM Inconel 718, and they propagate in a transgranular mode. Final fracture occurs in a ductile, dimpled mode.

To enhance the fatigue resistance of LENS Inconel 718, further improvements need to be made to the AM, or postmanufacturing, processes to more consistently produce parts with less porosity, inclusions, and more uniform microstructure.

ACKNOWLEDGEMENTS

REFERENCES

1. H. Krain, A. Sharman, and K. Ridgway, *J. Mater. Process. Technol.* 189, 153 (2007).
2. D. Dudzinski, *Int. J. Mach. Tool. Manuf.* 44, 439 (2004).
3. C.E. Leshock and J.N. Kim, *Int. J. Mach. Tool. Manuf.* 41, 877 (2001).
4. N. Shamsaei, A. Yadollahi, L. Bian, and S.M. Thompson, *Addit. Manuf.* 8, 12 (2015).
5. L. Bian, S.M. Thompson, and N. Shamsaei, *JOM* 67, 629 (2015).
6. A.J. Sterling, B. Torries, N. Shamsaei, S.M. Thompson, and D.W. Seely, *J. Mater. Sci. Eng. A* 655, 100 (2016).
7. E. Amsterdam and G.A. Kool, *ICAF Symp.* 1261 (2009).
8. R.I. Stephens, A. Fatemi, R.R. Stephens, and H.O. Fuchs, *Metal Fatigue in Engineering*, 2nd ed. (New York: Wiley, 2001), p. 106.
9. Q. Chen, N. Kawagoishi, and H. Nisitani, *J. Mater. Sci. Eng. A* 277, 250 (2000).
10. X. Ma, Z. Duan, H. Shi, R. Murai, and E. Yanagisawa, *J. Zhejiang Univ. Sci. A* 11, 727 (2010).
11. C. Mercer, A.B.O. Soboyejo, and W.O. Soboyejo, *J. Mater. Sci. Eng. A* 270, 308 (1999).
12. H. Andersson and C. Persson, *Int. J. Fatigue* 26, 211 (2004).
13. D.W. Worthem, I.M. Robertson, F.A. Leckie, D.F. Socie, and C.J. Alstetter, *Metall. Trans. A* 21, 3215 (1990).
14. C. Mercer, A.B.O. Soboyejo, and W.O. Soboyejo, *Acta Mater.* 47, 2727 (1999).
15. N. Kawagoishi, Q. Chen, and H. Nisitani, *Fatigue Fract. Eng. Mater. Struct.* 23, 209 (2000).
16. C. Brinkman and G.E. Korth, *J. Test. Eval.* 2, 249 (1974).
17. ASTM E606/E606 M-12, ASTM International, West Conshohocken, PA, 2012.
18. X. Zhao, J. Chen, X. Lin, and W. Huang, *J. Mater. Sci. Eng. A* 478, 119 (2008).
19. F. Liu, X. Lin, G. Yang, M. Song, J. Chen, and W. Huang, *Opt. Laser Technol.* 43, 208 (2011).
20. P.L. Blackwell, *J. Mater. Process. Technol.* 170, 240 (2005).
21. Y. Chen, F. Lu, K. Zhang, P. Nie, S.R.E. Hosseini, K. Feng, and Z. Li, *J. Alloys Compd.* 670, 312 (2016).
22. H. Qi, M. Azer, and A. Ritter, *Metall. Mater. Trans. A* 40, 2410 (2009).
23. L. Xiao, M.C. Chaturvedi, and D.L. Chen, *Metall. Mater. Trans. A* 36, 2671 (2005).